Acoustic focusing through two layer annuluses in air*

Yi-Jun Guan(管义钧)[1], Hong-Xiang Sun(孙宏祥)[1,2,†], Shu-Sen Liu(刘树森)[1], Shou-Qi Yuan(袁寿其)[1,‡], Jian-Ping Xia(夏建平)[1], and Yong Ge(葛勇)[1]

[1] *Research Center of Fluid Machinery Engineering and Technology, Jiangsu University, Zhenjiang* 212013, *China*
[2] *State Key Laboratory of Acoustics, Institute of Acoustics, Chinese Academy of Sciences, Beijing* 100190, *China*

(Received 3 April 2016; revised manuscript received 15 May 2016; published online 25 August 2016)

We report an acoustic focusing lens composed of two-layer annuluses made of metal cylinders in air. We find that the cylindrical waves can be focused into a perfect point without diffraction in the centre of the annuluses, which arises from the Mie-resonance modes in the annuluses. The focusing frequencies are related to the size of the inner annulus, and the focusing effect can be applied to the annuluses with different shapes and incident positions. Interesting applications of the focusing lens in the acoustic beam splitter and directional transmitter with energy enhancement are further discussed.

Keywords: acoustic focusing, metamaterials, annulus, cylinder

PACS: 43.35.+d, 43.20.+g **DOI:** 10.1088/1674-1056/25/10/104302

1. Introduction

The study on the acoustic focusing effect has attracted more and more attention, owing to its broad application prospects in many important fields, such as acoustic imaging, therapeutic ultrasound, and sonar systems. In the past few years, the emergence of acoustic metamaterials[1–10] has provided alternative solutions to acoustic lenses design. A variety of acoustic focusing lenses have been designed by the negative refraction mechanism, which can be mainly divided into two types: sonic crystals (SCs)[11–15] and acoustic metamaterials.[16–27]

By gradually changing the parameters of the SCs in the direction transverse to the acoustic propagation, such as the size,[11–13] elastic modulus,[12] shape,[14] and lattice spacing[15] of unit cells, the acoustic focusing effect is realized. However, the sizes of the SCs are all comparable to or larger than the wavelength, and therefore the sizes of these acoustic lenses are large at low frequency. The other type is acoustic metamaterials which are composed of a series of unit cells with different negative refractive indices, such as Helmholtz resonator,[16] cross structure,[17] coiling up space,[18,19,23] etc. A small and thin acoustic lens has become possible, owing to the small size and large negative refractive index of unit cell.

In addition to the aforementioned lenses, we have realized the acoustic focusing[28] and extraordinary acoustic transmission[29] by metal cylinder structures in water, which has potential applications in black box detectors in the sea and medical ultrasound treatment. However, the acoustic impedances of metal cylinders in the aforementioned work are much larger than that of air, thus it is hard to realize the focusing effect in the metal cylinders in air. In addition, the shapes of the metal cylinders cannot be adjusted at will, which apparently becomes an obstacle for practical applications of the focusing lenses.

In this work, we propose a linear acoustic focusing lens which is composed of two-layer annuluses made of cylinders immersed in air. The focusing effect arises from the Mie-resonance modes[30,31] in the annuluses. In addition, we investigate the acoustic focusing effect in the annulus structures with different sizes and shapes, and study the applications of the focusing lens in the acoustic beam splitter and directional transmitter with energy enhancement in detail.

2. System design and numerical results

2.1. System design

As schematically shown in Fig. 1(a), the acoustic focusing lens consists of two-layer annuluses made of brass cylinders immersed in air, and its cross section in the x–y plane is exhibited in Fig. 1(b) for convenience. The incident cylindrical source is located on the left side of the model. The inner (R_1) and outer (R_2) radii of the focusing lens (black dashed line region) are 13.0 mm and 22.5 mm, respectively, and the diameters of the inner (r_1) and outer (r_2) cylinders are 2.0 mm and 3.0 mm, respectively. Besides, the angle (θ) between two adjacent cylinders in both annuluses is 9° as indicated in Fig. 1(b).

*Project supported by the Major Program of the National Natural Science Foundation of China (Grant No. 51239005), the National Natural Science Foundation of China (Grant No. 11404147), the Natural Science Foundation of Jiangsu Province, China (Grant No. BK20140519), the China Postdoctoral Science Foundation (Grant No. 2015M571672), the Research Fund for Advanced Talents of Jiangsu University, China (Grant No. 11JDG118), and the Training Project of Young Backbone Teachers of Jiangsu University, China.

†Corresponding author. E-mail: jsdxshx@ujs.edu.cn
‡Corresponding author. E-mail: Shouqiy@ujs.edu.cn

© 2016 Chinese Physical Society and IOP Publishing Ltd

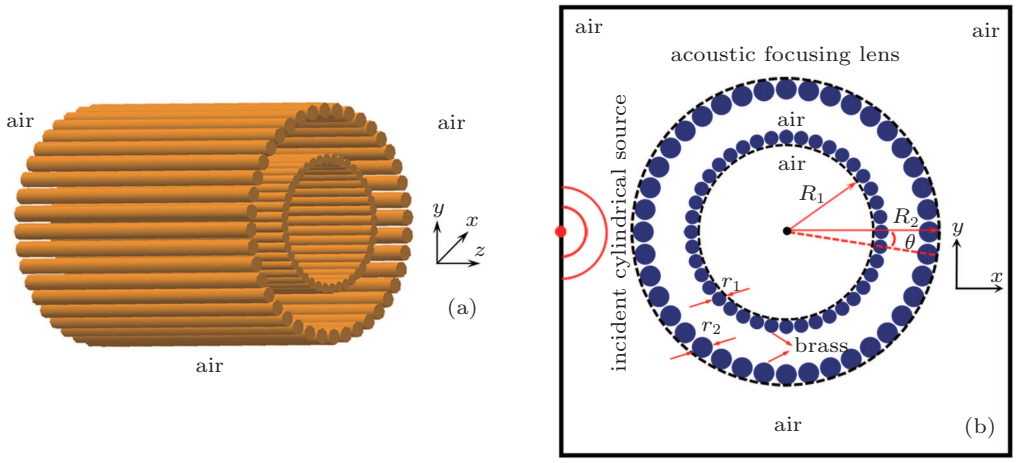


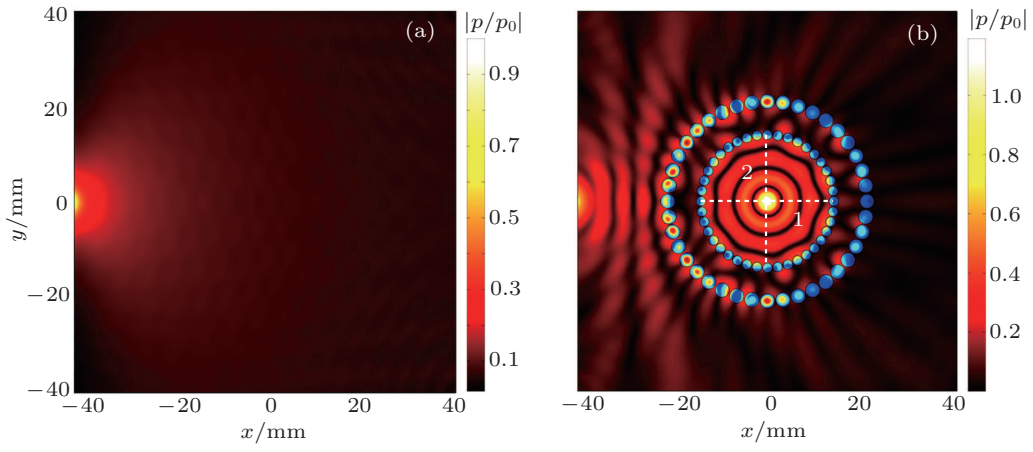
Fig. 1. (color online) (a) Schematic diagram of acoustic focusing lens and (b) cross section in the x–y plane.

Throughout this work, the focusing characteristics of the focusing lens are numerically simulated by the finite element method based on COMSOL Multiphysics software, and the material parameters are listed as follows: the density $\rho_b = 8400$ kg/m^3, the longitudinal wave velocity $c_l = 4400$ m/s, and the transversal wave velocity $c_s = 2200$ m/s for brass; $\rho_w = 1.21$ kg/m^3 and $c_w = 344$ m/s for air. In the simulations, the acoustic-structure boundary conditions are imposed on the boundaries of each brass cylinder.

2.2. Focusing characteristics

Figures 2(a) and 2(b) exhibit the amplitude distributions ($|p/p_0|$) of the pressure fields for the free space and the focusing lens at 42.63 kHz, respectively. The incident cylindrical source is located at (−40 mm, 0) in Cartesian coordinates, and its initial amplitude $|p_0|$ is 1.0 Pa. As shown in Fig. 2(a), in the free space, the cylindrical wave is attenuated rapidly with the increase of the propagation distance. However, with the focusing lens, the cylindrical wave is focused into a perfect point without diffraction at the center of the annuluses, which is shown in Fig. 2(b). Moreover, the focusing effect also exists at many other frequencies, such as 29.50 kHz and 55.32 kHz, which are shown in Figs. 2(c) and 2(d). It also presents great focusing performance at these frequencies. By comparing the results in Figs. 2(b)–2(d), we find that the size of the focal spot becomes smaller with the increase of the frequency due to the wavelength of the cylindrical wave. Figures 2(e) and 2(f) show the focusing characteristics in the lens with different layer numbers, and the other parameters are the same as those in Fig. 2(b). As shown in Figs. 2(e) and 2(f), the focusing effect also exists. Compared with the scenario in Fig. 2(b), the focusing effect is much weaker for the single layer lens, but is almost the same for the three layer lens. The maximum values of $|p/p_0|$ at the focal spot are 0.43, 1.19, and 1.22 in Figs. 2(e), 2(b), and 2(f), respectively. Therefore, we design two-layer annuluses in the acoustic focusing lens.

Figures 3(a) and 3(b) present the longitudinal and transverse profiles of the pressure amplitudes passing through the focal spots in Fig. 2(b), and the pressure profiles in the free space are plotted there for comparison. Note that the focusing effects exist in both the x and the y directions, and the width of the focal spot in the x direction is $\lambda/2$, which is the same as that in the y direction. Moreover, compared with the results in the free space, the amplitude at the focal spot is enhanced by about 12 times, with using the annuluses. The aforementioned results indicate that the great focusing effect is realized by the two-layer annuluses in air.



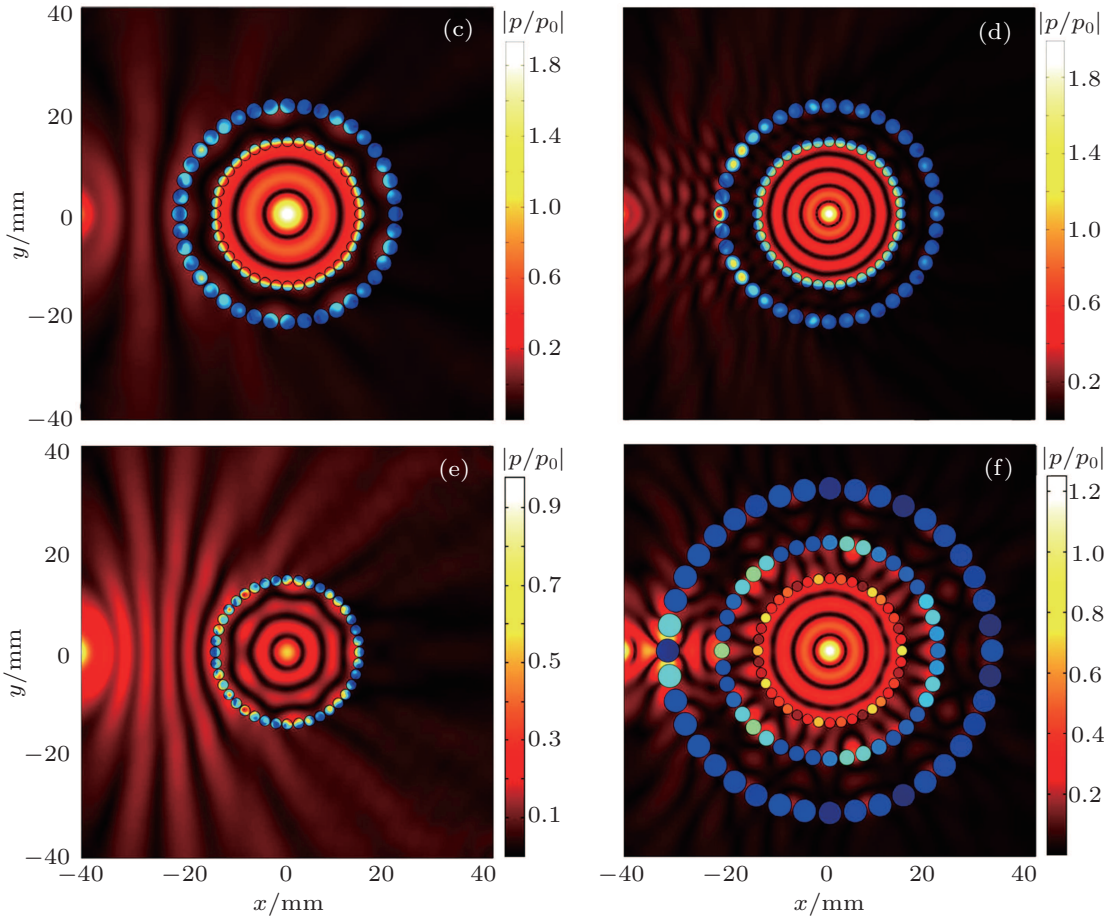


Fig. 2. (color online) Pressure–field amplitude patterns for (a) free space at 42.63 kHz and focusing lenses with two-layer annuluses at (b) 42.63 kHz, (c) 29.50 kHz, and (d) 55.32 kHz, with (e) single layer annulus at 42.51 kHz, and with (e) three-layer annuluse at 42.59 kHz, respectively.

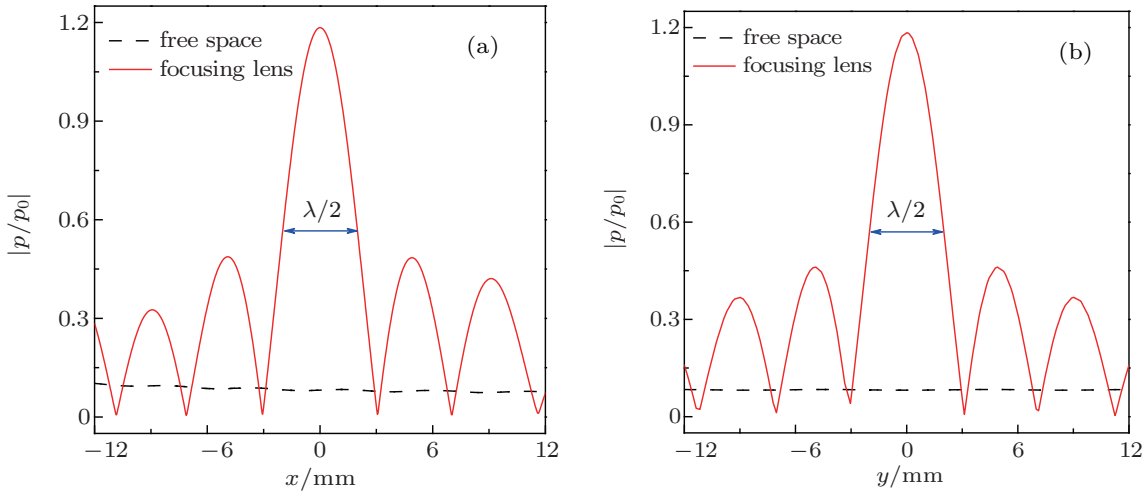


Fig. 3. (color online) Pressure amplitude distributions along a line passing through focal spot (a) in the propagation direction and (b) in a direction transverse to the propagation direction (shown as lines "1" and "2" in Fig. 2(b)).

2.3. Verification of focusing lens

In order to verify the performance of the focusing lens, we establish the simplified model composed of a cylinder structure immersed in air, which is shown in Fig. 4(a), and the parameters R_1 and R_2 are the same as those in Fig. 1(b). The absolute value of the acoustic velocity $|v_{\text{eff}}|$ and the real part of the density ρ_{eff} of the effective medium are shown in Fig. 4(b), and the two parameters are numerically calculated from the complex reflection and transmission coefficients.[32] Figure 4(c) presents the amplitude distribution of the pressure field for the simplified model at 42.63 kHz, and the focusing characteristics are very similar to those in the focusing lens [Fig. 2(b)], indicating the validity of the proposed focusing lens.

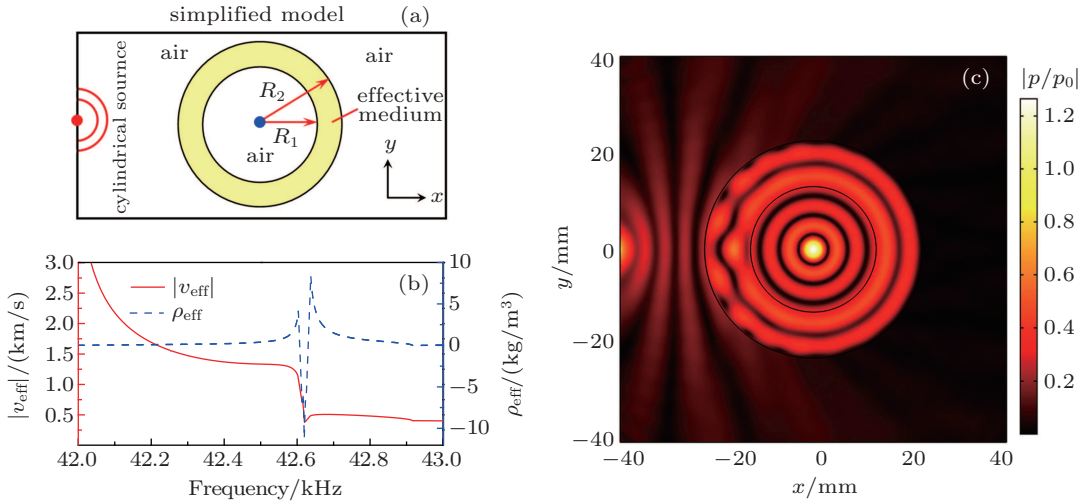


Fig. 4. (color online) (a) Schematic diagram of the simplified model, and (b) the real part of effective density ρ_{eff} and the absolute value of effective acoustic velocity $|v_{\text{eff}}|$ each as a function of frequency. (c) Pressure field amplitude pattern for the simplified model at 42.63 kHz.

2.4. Mechanism of focusing lens

Figures 5(a)–5(c) show the phase distributions of the pressure fields, which correspond to Figs. 2(a), 2(b), and 4(c), respectively. We find that the phase waveforms are a series of undisturbed circular lines in the free space [Fig. 5(a)]. However, it is found from Figs. 5(b) and 5(c) that the phase distributions are reconstructed inside the annuluses, and the phase waveforms are transformed into a series of concentric circles with the same values and eventually focus into a point in the centre of the annuluses.

To obtain an insight into the mechanism of the focusing effect, we simulate the deformation of the total displacement distributions in the annuluses in Fig. 2(b), of which the result is shown in Fig. 5(d). It is found from Fig. 5(d) that the Mie-resonance mode [30,31] is excited in the annuluses at an eigenfrequency of 43.62 kHz, and the vibration directions (indicated by red arrows) pointing to the focal spot, especially those in the inside annulus. It is deduced that the propagation directions of the cylindrical wave are restructured by the Mie-resonance mode, and the cylindrical waves are finally focused into a perfect point in the center of the annuluses.

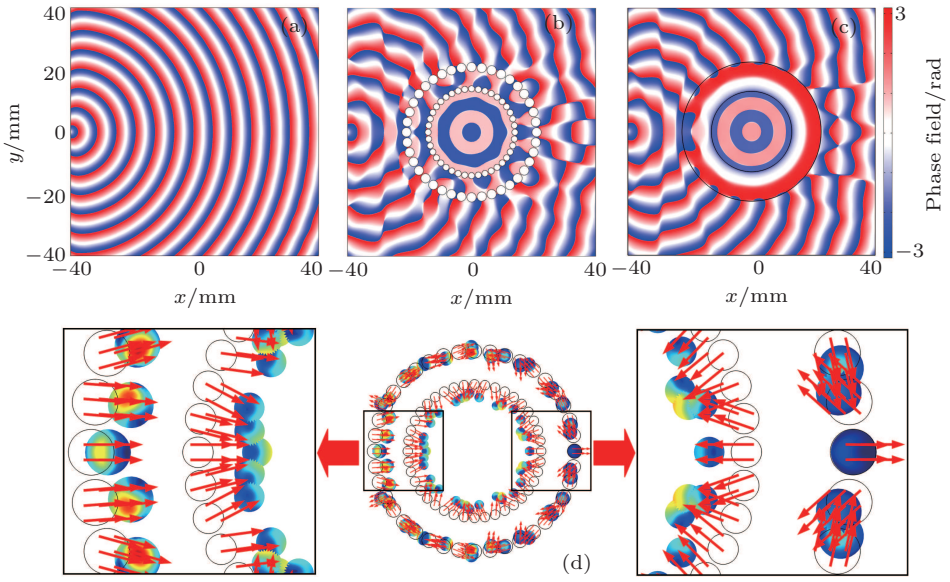


Fig. 5. (color online) Pressure field phase patterns for (a) free space, (b) focusing lens, and (c) the simplified model at 42.63 kHz, and (d) deformation of total displacement field pattern in annuluses, with red arrows representing vibration directions of displacements.

3. Influences of parameters of annuluses on focusing effect

3.1. Size of annuluses

We simulate the amplitude distributions of the pressure fields by magnifying all the sizes of the outer annulus (R_2 and r_2) and inner annulus (R_1 and r_1) n times. From Figs. 6(a)–6(h), we find that the focusing frequencies are almost the same for different size outer annuluses [Figs. 6(a)–6(d)], but are inversely proportional to the size of the inner annulus [Figs. 6(e)–6(h)]. It indicates that the focusing frequency is closely related to the size of the inner annulus.

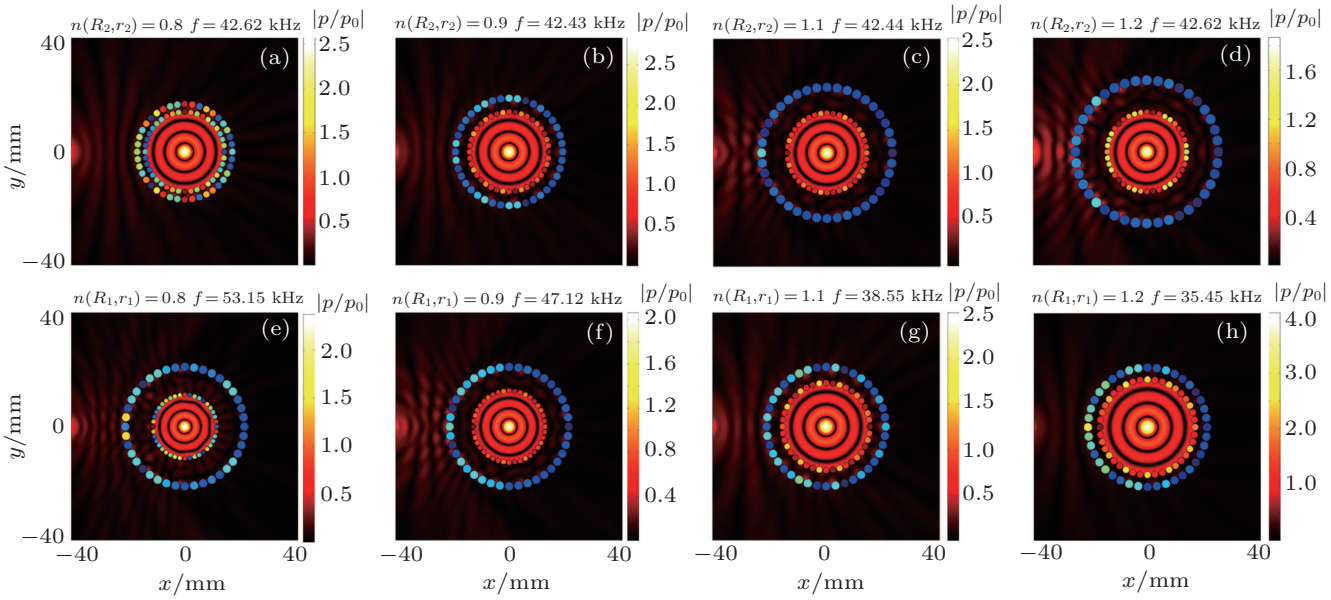


Fig. 6. (color online) Pressure–field amplitude patterns for focusing lens by magnifying the parameters ((a)–(d)) R_2 and r_2 and ((e)–(h)) R_1 and r_1 n times.

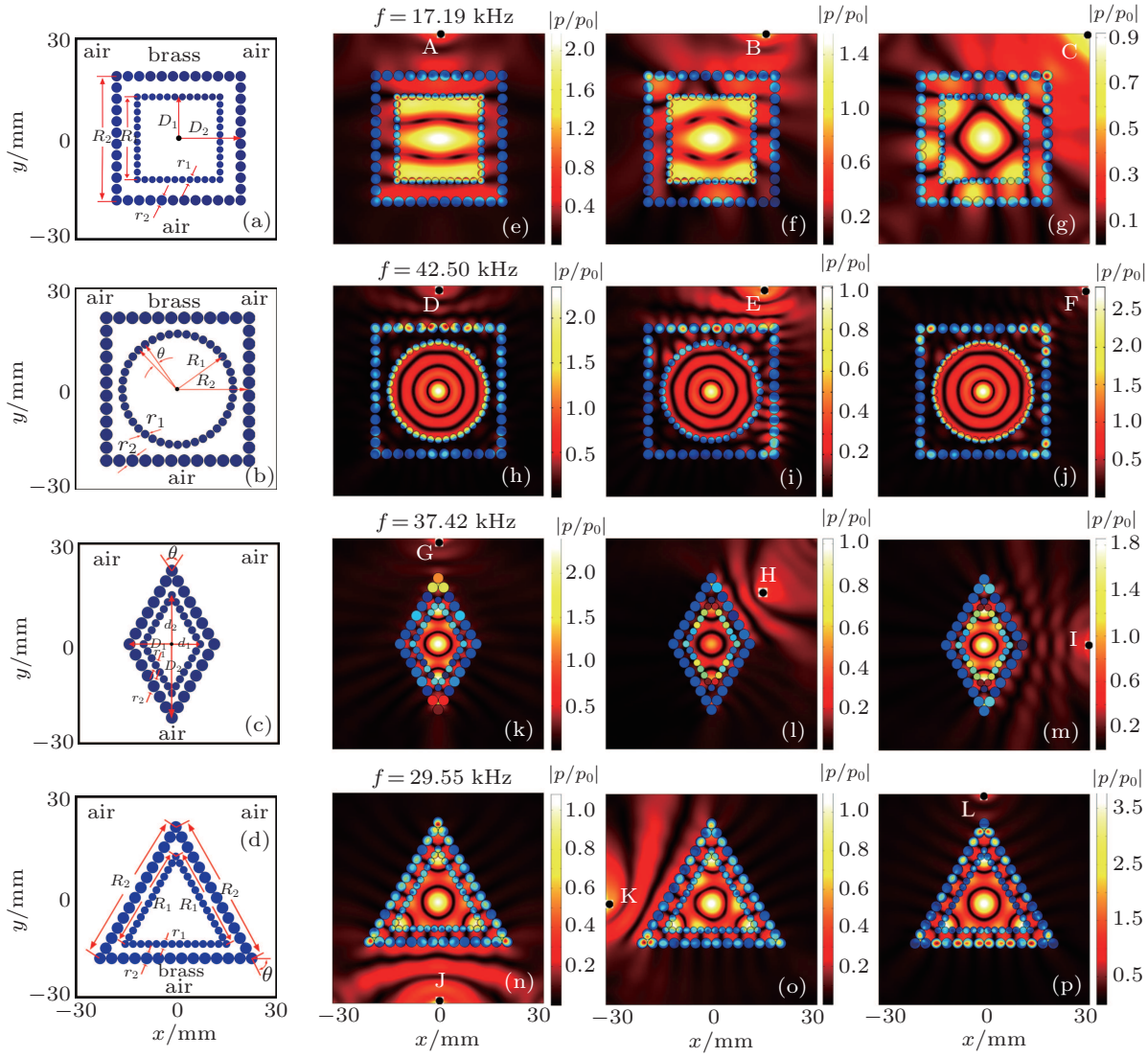


Fig. 7. (color online) Schematic diagrams of (a) square annuluses ($R_1 = 24.00$ mm, $R_2 = 36.00$ mm, $D_1 = 12.00$ mm, $D_2 = 18.00$ mm, $r_1 = 2.00$ mm, and $r_2 = 3.00$ mm), (b) square and circular annuluses ($\theta = 9°$, $R_1 = 14.00$ mm, $R_2 = 18.00$ mm, $D_1 = 12.00$ mm, $D_2 = 18.00$ mm, $r_1 = 2.00$ mm, and $r_2 = 3.00$ mm), (c) rhomboic annuluses ($\theta = 60°$, $d_1 = 7.22$ mm, $d_2 = 12.50$ mm, $D_1 = 10.83$ mm, $D_2 = 18.75$ mm, $r_1 = 2.00$ mm, and $r_2 = 3.00$ mm), and (d) triangular annuluses ($R_1 = 26.27$ mm, $R_2 = 39.40$ mm, $r_1 = 2.00$ mm, $r_2 = 3.00$ mm, and $\theta = 60°$). Pressure–field amplitude patterns for ((e)–(g)) square annuluses, ((h)–(j)) square and circular annuluses, ((k)–(m)) rhomboic annuluses, and ((n)–(p)) triangular annuluses with different incident positions.

3.2. Shape of annuluses

Furthermore, we find that the focusing effect exists in different shaped annulus structures. To verify the feasibility of this case, we design four types of annuluses with different shapes immersed in air, which are shown in Figs. 7(a)–7(d). As shown in Figs. 7(e)–7(p), the cylindrical waves are focused into the four different-annulus structures at 17.19, 42.50, 37.42, and 29.55 kHz, respectively, and note that the incident cylindrical waves are located at different positions outside the annuluses.

4. Potential applications of focusing effect

4.1. Acoustic beam splitter

The focusing effect on the annuluses has substantial practical significance in the acoustic beam splitter in air. As is well known, the energies of acoustic waves are divided into several portions and reduce greatly in the traditional beam splitters. Here, we propose an acoustic beam splitter with the energy enhancement by using annulus structures shown in Fig. 7(a), but the incident cylindrical wave is located in the center of the annulus structure, and its initial amplitude $|p_0|$ is also 1.0 Pa. Besides, the amplitude distribution of the pressure field in free space is also calculated for comparison as shown in Fig. 8(a), in which the white circular lines represent the contour lines of the amplitude ($|p/p_0|$). It is found from Fig. 8(b) that the output waves are divided into four acoustic beams. Compared with the result in Fig. 8(a), the amplitude at the exciting point is enhanced by about 40 times, and the amplitude of each beam through the annuluses is increased by about 15 times (Fig. 8(b)). To clearly exhibit the characteristics of the output waves, we magnify the pressure field outside the annuluses with different color bar and plot it in Fig. 8(c), and the amplitudes of the output waves are larger than those in free space.

4.2. Acoustic directional transmitter

Furthermore, we consider the annulus structure [Fig. 7(a)] surrounded by a square annulus structure with an opening on an edge, which is schematically shown in Fig. 8(d). Figure 8(e) shows the amplitude distribution of the pressure field for this structure, where the energies of the output waves through the opening are concentrated in one direction. Compared with Fig. 8(b), figure 8(e) shows that the amplitude of the output waves is magnified 1.5 times, which is also clearly shown in Fig. 8(f). This effect may have potential applications in acoustic directional transmitters.

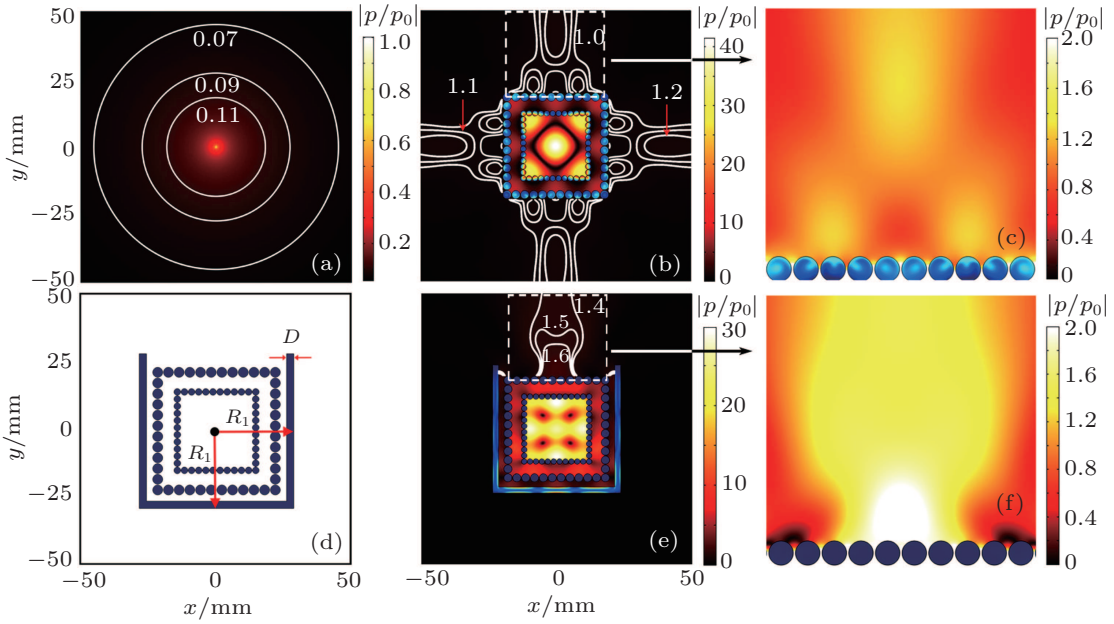


Fig. 8. (color online) Pressure–field amplitude patterns for (a) free space and (b) square annuluses at 17.19 kHz, and (c) partial zoom in panel (b). (d) Schematic diagram of acoustic directional transmitter ($R_1 = 23.50$ mm, and $D = 2.00$ mm). (e) Pressure–field amplitude pattern for acoustic directional transmitter at 17.19 kHz, and (f) partial zoom in panel (e). White circular lines represent contour lines of amplitude.

5. Conclusions

In this work, we realize the acoustic focusing effect through two-layer annuluses made of brass cylinders immersed in air. The numerical results show that the cylindrical waves can be focused into a perfect point without diffraction, and the focusing effect arises from the Mie-resonance modes in the annulus structure, which is different from the focusing lenses realized by the negative refraction mechanism. More importantly, we find that the focusing frequency is closely related to the size of the inner annulus, and the focusing effect can be applied to the annulus structures with different shapes and incident positions. Prospective applications of the focusing effect in the acoustic beam splitter and directional transmitter are investigated in detail, and the amplitude of the out-

put beam is magnified greatly (at least 15 times). Our finding should have a contribution to ultrasonic applications.

References

[1] Liu Z Y, Zhang X X, Mao Y W, Zhu Y Y, Yang Z Y, Chan C T and Sheng P 2000 *Science* **289** 1734
[2] Li J and Chan C T 2004 *Phys. Rev. E* **70** 055602
[3] Fang N, Xi D, Xu J, Ambati M, Srituravanich W, Sun C and Zhang X 2006 *Nat. Mater.* **5** 452
[4] Lu M H, Liu X K, Feng L, Li J, Huang C P and Chen Y F 2007 *Phys. Rev. Lett.* **99** 174301
[5] Li J, Fok L, Yin X, Bartal G and Zhang X 2009 *Nat. Mater.* **8** 931
[6] Liang B, Yuan B and Cheng J C 2009 *Phys. Rev. Lett.* **103** 104301
[7] Liang Z and Li J 2012 *Phys. Rev. Lett.* **108** 114301
[8] Fleury R, Sounas D L, Sieck C F, Haberman M R and Alù A 2014 *Science* **343** 516
[9] Xie Y B, Wang W Q, Chen H Y, Konneker A, Popa B I and Cummer S A 2014 *Nat. Commun.* **5** 5553
[10] Duan Y T, Luo J, Wang G H, Hang Z H, Hou B, Li J, Sheng P and Lai Y 2015 *Sci. Rep.* **5** 12139
[11] Deng K, Ding Y Q, He Z J, Zhao H P, Shi J and Liu Z Y 2009 *J. Phys. D: Appl. Phys.* **42** 185505
[12] Lin S C S, Huang T J, Sun J H and Wu T T 2009 *Phys. Rev. B* **79** 094302
[13] Climente A, Torrent D and Sánchez-Dehesa J 2010 *Appl. Phys. Lett.* **97** 104103
[14] Torrent D and Sánchez-Dehesa J 2007 *New J. Phys.* **9** 323
[15] Peng S S, He Z J, Jia H, Zhang A Q, Qiu C Y, Ke M Z and Liu Z Y 2010 *Appl. Phys. Lett.* **96** 263502
[16] Zhang S, Yin L L and Fang N 2009 *Phys. Rev. Lett.* **102** 194301
[17] Zigoneanu L, Popa B -I and Cummer S A 2011 *Phys. Rev. B* **84** 024305
[18] Li Y, Liang B, Tao X, Zhu X F, Zou X Y and Cheng J C 2012 *Appl. Phys. Lett.* **101** 233508
[19] Li Y, Liang B, Gu Z M, Zou X Y and Cheng J C 2013 *Sci. Rep.* **3** 2546
[20] Hladky-Hennion A C, Vasseur J O, Haw G, Croënne C, Haumesser L and Norris A N 2013 *Appl. Phys. Lett.* **102** 144103
[21] Molerón M, Serra-Garcia M and Daraio C 2014 *Appl. Phys. Lett.* **105** 114109
[22] Tang K, Qiu C Y, Lu J Y, Ke M Z and Liu Z Y 2015 *J. Appl. Phys.* **117** 024503
[23] Yuan B G, Cheng Y and Liu X J 2015 *Appl. Phys. Express* **8** 027301
[24] Tian Y, Wei Q, Cheng Y, Xu Z and Liu X J 2015 *Appl. Phys. Lett.* **107** 221906
[25] Zhou L, Guo X S, Tu J, Ma Q Y, Wu J R and Zhang D 2015 *J. Appl. Phys.* **117** 104503
[26] Gao H, Gu Z M, Liang B, Zou X Y, Yang J, Yang J and Cheng J C 2016 *Appl. Phys. Lett.* **108** 073501
[27] Liu C, Sun H X, Yuan S Q and Xia J P 2016 *Acta Phys. Sin.* **65** 044303 (in Chinese)
[28] Xia J P and Sun H X 2015 *Appl. Phys. Lett.* **106** 063505
[29] Xia J P, Sun H X, Yuan S Q and Zhang S Y 2015 *Appl. Phys. Express* **8** 104301
[30] Cheng Y, Zhou C, Yuan B G, Wu D J, Wei Q and Liu X J 2015 *Nat. Mater.* **14** 1013
[31] Xia J P, Sun H X, Cheng Q, Xu Z, Chen H, Yuan S Q, Zhang S Y, Ge Y and Guan YJ 2016 *Appl. Phys. Express* **9** 057301
[32] Fokin V, Ambati M, Sun C and Zhang X 2007 *Phys. Rev. B* **76** 144302